Wave Dynamics and Sediment Transport in Great Salt Lake: A Model-Data Comparison

Benjamin Smith[1], Robert Mahon[2], Tyler Lincoln[3], Cedric J. Hagen[4], Juliana Olsen-Valdez[3], John Magyar[1], and Elizabeth Trower[3]

[1]*Division of Geological and Planetary Sciences, California Institute of Technology, Pasadena, California, bpsmith@caltech.edu*
[2]*Department of Earth and Environmental Sciences, University of New Orleans, New Orleans, Louisiana*
[3]*Department of Geological Sciences, University of Colorado Boulder, Boulder, Colorado, Lizzy.Trower@colorado.edu*
[4]*Department of Geosciences, Princeton University, Princeton, New Jersey*

10.31711/ugap.v51i.139

ABSTRACT

Great Salt Lake is a natural laboratory to test and refine ideas about the relationship between sediment transport by waves and the characteristics of shoreline carbonate sediments, in particular ooid sands and microbialite mounds. In this chapter, we present a year-long series of wave data collected from July 2021 through June 2022 and use these wave data to assess the performance of a US Army Corps of Engineers wave model previously used to estimate bed shear velocity and intermittency of sediment transport in Great Salt Lake (Smith and others, 2020). We use this model-data comparison to identify the strengths and weaknesses of the existing model for both geological and ecological applications, and areas of improvement for future model development. We also use shallow sediment cores and Unmanned Aerial Vehicle (UAV)-based orthomosaics collected from shorelines near each buoy to assess how the wave climate along two parts of the lake shore influences the stratigraphic record and the surface morphology of the lakebed.

INTRODUCTION

Great Salt Lake (GSL), UT is a critical ecological and economic resource—a key waypoint in the Pacific flyway (Paul & Manning, 2002) and a primary source of magnesium metal in North America (Tripp, 2009). GSL is also home to an exceptional modern geobiological archive of at least1000 km^2 of meter-scale microbialite mounds (Vanden Berg, 2019; Baskin and others, 2021) that play a key role in the GSL ecosystem (Wurtsbaugh and others, 2011). These mounds act as a food source and substrate critical for reproduction cycles for the brine fly, *Ephydra gracilis,* and the brine shrimp, *Artemia franciscana,* which in turn are key food sources for the millions of shorebirds and waterbirds that visit GSL each year (Collins, 1980; Wurtsbaugh, 2009; Belovsky and others, 2011). Radiocarbon dating, though complex, suggests that GSL microbialites have been accumulating for >10,000 years (Bouton and others, 2016a; Newell and others, 2017, 2020; Homewood and others, 2022). Previous authors have described gradients in microbialite morphology with distance from the shoreline and/or water depth (Eardley, 1938; Carozzi, 1962; Bouton and others, 2016a, 2016b; Vanden Berg, 2019), suggesting that hydrodynamics and sediment transport, in addition to geochemistry and microbial metabolic activity, play a role in microbialite construction. Previous workers have also observed that elongated microbialite mounds or domes tend to have preferred orientations relative to a shoreline and/or wave crests (Bouton and others, 2016a; Chidsey and others, 2015; Vanden Berg, 2019). These observations hint at a potential link between sediment transport and microbialite morphology and orientation. In theory, GSL microbialites are an ideal system in which to test ideas about the role of hydrodynamics and sediment transport on microbialite morphology because microbialites occur along shorelines with different orientations and therefore experience different wave conditions. However, this work first requires a more robust understanding of wave dynamics in the lake and an ability to accurately model past wave conditions (e.g., prior to causeway construction and at higher lake levels) along different shorelines.

Beyond microbialites, wave dynamics in the lake also affect other sedimentological and ecological characteristics of the lake. For example, the formation (including grain size and shape) of ooids is influenced by the frequency and energy of sediment transport (Trower and others, 2020). Wave dynamics can also influence mixing of the typically-stratified South Arm lake water, which in turn affects the ecosystem by varying the availability and mobility of nutrients (Belovsky and others, 2011) and delivery of toxins like mercury, selenium, and arsenic from the deep brine layer to the upper water column (Beisner and others, 2009; Jones and Wurtsbaugh, 2014). Furthermore,

given the historically low lake levels witnessed in 2021 and 2022 (Abbott and others, 2023), accurate models of wave climate are needed to better understand how different future lake levels (higher or lower) will influence the hydrodynamics of the ecosystem.

Previously, Trower and others (2020) and Smith and others (2020) applied a linear wave model (Rohweder and others, 2008) to calculate wave characteristics and bed shear stress using GSL bathymetry (Baskin and Allen, 2005; Baskin and Turner, 2006; Tarboton, 2017) and wind data from the University of Utah MesoWest database (Horel and others, 2002). However, this model was not necessarily designed to perform optimally for an environment like GSL, which includes very shallow and low sloping shorelines and the sharp changes in shoreline slope associated with the East Lake fault scarp off the western shore of Antelope Island (Colman and others, 2002). The purpose of this paper is to assess the performance of a linear wave model in GSL using data from two wave buoys in parts of the lake with contrasting shoreline orientations. -We evaluated the performance of this linear wave model using data from these wave buoys. We also present observations from sediment cores collected near each wave buoy and measurements of microbialite orientations adjacent to one wave buoy to assess how wave climate affects the composition and morphology of carbonate sediments along differently-oriented shorelines. Our ultimate goal is to assess whether the model performs sufficiently well to be more widely applied to predict future and/or reconstruct ancient wave hydrodynamics in GSL.

METHODS

Wind and Wave Measurements

SoFarOcean Spotter wave buoys were deployed at two locations along the South Arm of the lake from the period of July 13, 2021, through June 28, 2022 (Figure 1). The two sites were selected based on public interest and scientific importance. Buoy #1356 (Black Rock) was deployed near GSL State Park and buoy #1328 (Miera Spit) was deployed near the southern end of Antelope Island State Park. Previous work documented relationships between sedimentary facies and the physical environment near these locations, including Trower and others (2020) with ooids near Black Rock, and Smith and others (2020) with rip-up clasts and other storm features near Miera Spit. Both buoys were deployed in relatively shallow water, approximately 2.5 m for #1356 and 1.6 m for #1328. For each wave buoy, water depth was measured using HOBO U20L-04 water level loggers attached to anchors. Each logger recorded pressure and temperature every 30 minutes; pressure measurements from each logger were converted to water depth using a water density of 1100 kg/m^3 and corrected for atmospheric pressure using data from the KCC01 MesoWest weather station.

SoFarOcean buoys were chosen for deployment because they offer a lower-cost alternative to other wave monitoring techniques, and they transmit in real time through the use of onboard accelerometers and Iridium satellite communication capabilities. Buoys operated in six-hour cycles, alternating 5 hours of rest with one hour of active data collection. At the end of each cycle, buoys performed onboard processing of accelerometer data, converting it to spectral wave parameters—e.g., significant wave height, peak and mean direction, and spectral moments using open-source algorithms made available by SoFarOcean. At the end of the study, higher-frequency data were retrieved from the buoy's onboard memory and processed using SoFarOcean parsing and analysis scripts (parser_v1.12.0). The full dataset for both buoys is available in an online repository (Mahon and others, 2023), including additional wave data (e.g., directional spread, etc.) and metadata (e.g., temperature) not directly described in this chapter.

For each buoy, HOBO water depth time series data were examined to determine whether the anchors moved during the study period, as evidenced by substantial step changes in water depth. Water depths for #1356 (Black Rock) varied smoothly between 1.73-2.95 m, reaching a low point of 1.73 m in October 2021, corresponding to the new historical low of 4190.1 ft (Figure 2). Buoy #1356 (Black Rock) was retrieved in good working order with no evidence of anchor movement or onboard electronics failures, indicating that the buoy made reliable wave measurements over the full study period. In contrast, water depths for #1328 (Miera Spit) started at 1.78 m but dropped rapidly to 0.85m on July 15, 2021, and dropped further to 0.43m on August 17, 2021 (Figure 2). The timing of these rapid water depth changes matches the timing of buoy location changes when the anchor was dragged inshore by waves. When buoy #1328 (Miera Spit) was retrieved at the end of the study period, it was partially beached with its ballast chain touching the bed. We surmised that data quality was suspect after the second abrupt change in water depth on August 17, 2021, when the anchor was moved during a storm. A second consideration to buoy data quality was the detection limit of very low-amplitude waves. Under calm conditions, buoy sensors experience an internal electronic "ringing" which produces spurious derived wave data with unrelated

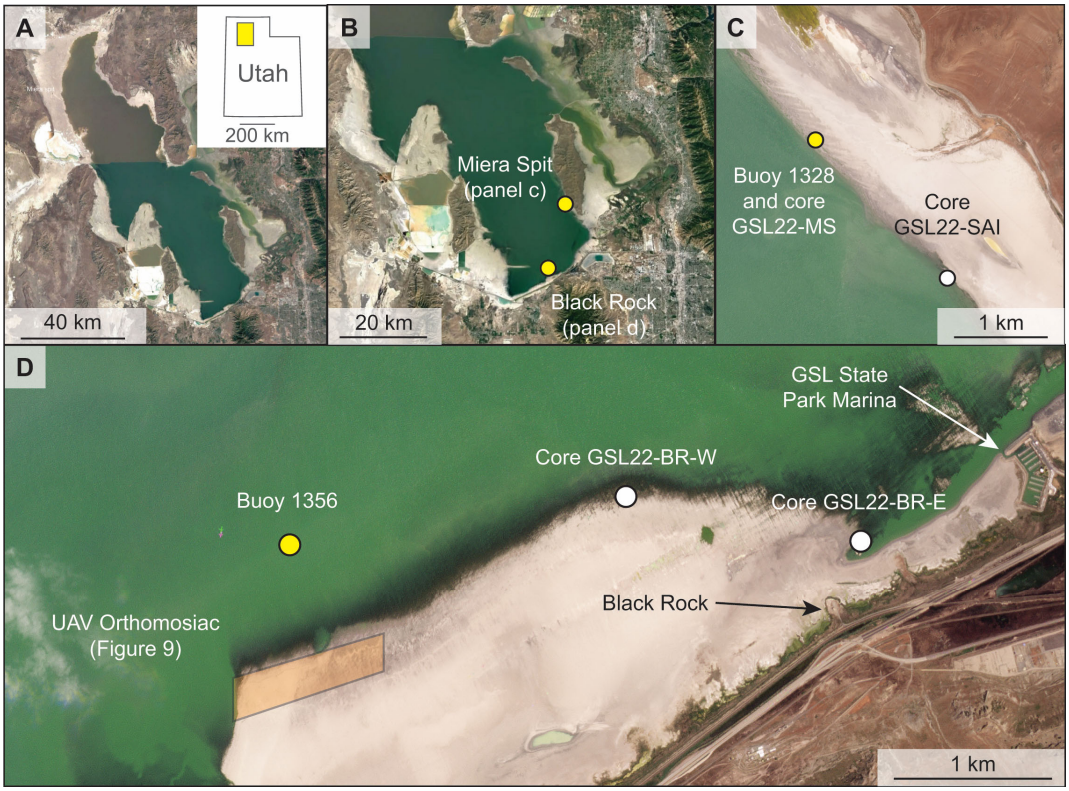

Figure 1. *The GSL-BB system. A. Location of GSL and Lake Bonneville in western Utah. B. Overview map of GSL showing the historic average elevation, and the new 2022 historic low (Figure from Clark and Baxter, 2023.) C. Corresponding Landsat satellite imagery of GSL elevations showing the record high of GSL in 1986 at left vs. historic low in 2022. AI = Antelope Island. Images (Images are public domain.) D. Known Bonneville basin lake cycles. The blue line labeled B in the main graph marks the Bonneville deep-lake cycle. Vertical black bars represent older deep-lake cycles. The base of the main graph is the elevation of modern GSL. Inset shows the shoreline history of Lake Bonneville (blue) and GSL (red) with named shorelines (also see Figure 3). (Inset figure from Oviatt and Shroder, 2016a).*

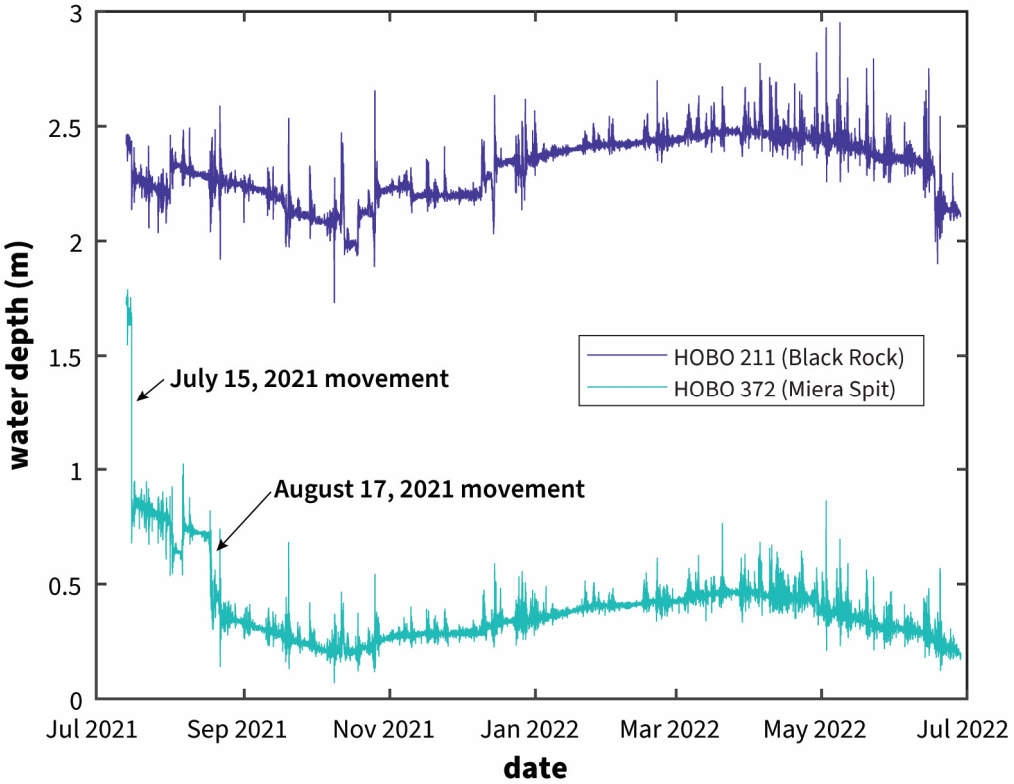

Figure 2. *Logs of water depth at each buoy location over the year-long deployment. Note abrupt drops in water depth at Miera Spit buoy on July 15, 2021 and August 17, 2021. These correspond with storm events and affect data quality after July 15th.*

directions and magnitudes. These data were distinguished by their long periods (up to 20s) which were unreasonable for waves in the lake. From the 1400 wave spectral records at buoy #1356 (Black Rock), 793 were deemed to accurately reflect present conditions based on their wave periods (<10s). For buoy #1328 (Miera Spit), 41 records were deemed suitable based on the abbreviated operation period and noise screening.

Wind speed and direction were obtained from several wind stations in the MesoWest database over a period coinciding with buoy deployment (7-13-2021 to 6-28-2022, Figure 3). For both wind/wave comparisons and fetch-limited calculations, stations were selected based on proximity to each buoy and completeness of wind data over the study period. Wind conditions near buoy #1356 (Black Rock) were taken from station KCC02, located in the marina of GSL State Park (Figure 3). Wind conditions near buoy #1328 (Miera Spit) were taken from the station at Hat Island (HATUT) because other, more proximal stations either had incomplete records or were not operational over the study period.

Comparing Estimated and Observed Wave Parameters

Wave parameters can be estimated using a combination of linear wave theory, empirically derived equations, and measurements for wind speed and fetch. Many studies use methods developed by the US Army Corps of Engineers as outlined in the Coastal Engineering Manual (U.S. Army Corps of Engineers, 2002) and the Shore Protection Manual (Coastal Engineering Research Center, 1984). In particular, this approach underlies recent work by Trower and others (2020) and Smith and others (2020) which used an ArcGIS plugin (Rohweder and others, 2008) to estimate wave parameters based on MesoWest wind data (Horel and others, 2002) and a digital elevation model (Tarboton, 2017). A comparison between observed and calculated wave parameters provides direct feedback on the appropriateness of commonly used approaches for GSL, as well as potential complications due to wave refractions/diffraction, interactions with lake bathymetry, and inaccuracy of the bathymetry model.

The model-data comparisons focused on significant wave heights, peak wave heights, and estimated shear velocities at the bed. Significant wave heights, defined as the average height of the upper one-third of wave crests, were calculated using a procedure used in the Coastal Engineering Manual for fetch-limited conditions (U.S. Army Corps of Engineers, 2002):

$$C_d = 0.001 * (1.1 + (0.035 * U_A) \quad (1)$$

$$U^* = (C_d)^{1/2} * U_A \quad (2)$$

$$\hat{x} = (g * x)/(U^*)^2 \quad (3)$$

$$\hat{H}_{m0} = \lambda_1 * (\hat{x})^{m1} \quad (4)$$

$$H_{m0} = \hat{H}_{m0} * (U^*)^2/g \quad (5)$$

where C_d is the drag coefficient, U_A is the wind speed (m/s) adjusted for height and whether the observations were collected over land or water, U^* is the friction velocity (m/s), x is the wind fetch, $\hat{x}$ is the non-dimensional wind fetch, $\hat{H}_{m0}$ is the non-dimensional significant wave height, H_{m0} is the significant wave height (m), λ_1 is a constant with a value of 0.0413, g is gravitational acceleration (9.81 m/s^2), and m_1 is a constant with a value of ½.

Peak wave periods under fetch-limited conditions were calculated using:

$$\hat{T}_p = \lambda_2 * (\hat{x})^{m2} \quad (6)$$

$$T_p = \hat{T}_p * U^*/g \quad (7)$$

where $\hat{T}_p$ is the non-dimensional peak wave period, λ_2 is a constant with a value of 0.751, m_2 is a constant with a value of ⅓, and T_p is the peak wave period.

Shear velocities were calculated using estimates of maximum orbital velocity and wavelength as intermediate steps. Wavelengths (L) were calculated as:

$$L = gT^2_p * 2\pi \quad (8)$$

and maximum orbital velocities, u_m, were calculated as:

$$u_m = \pi H_{m0}/(T_p \sinh(2\pi d_f/L)) \quad (9)$$

Shear velocities, u_*, were calculated as:

$$u_*^2 = 1/2\, f\, u_m \quad (10)$$

where f is the friction factor set to 0.032. Note that while significant wave height and wave period provide direct comparisons between model estimates and

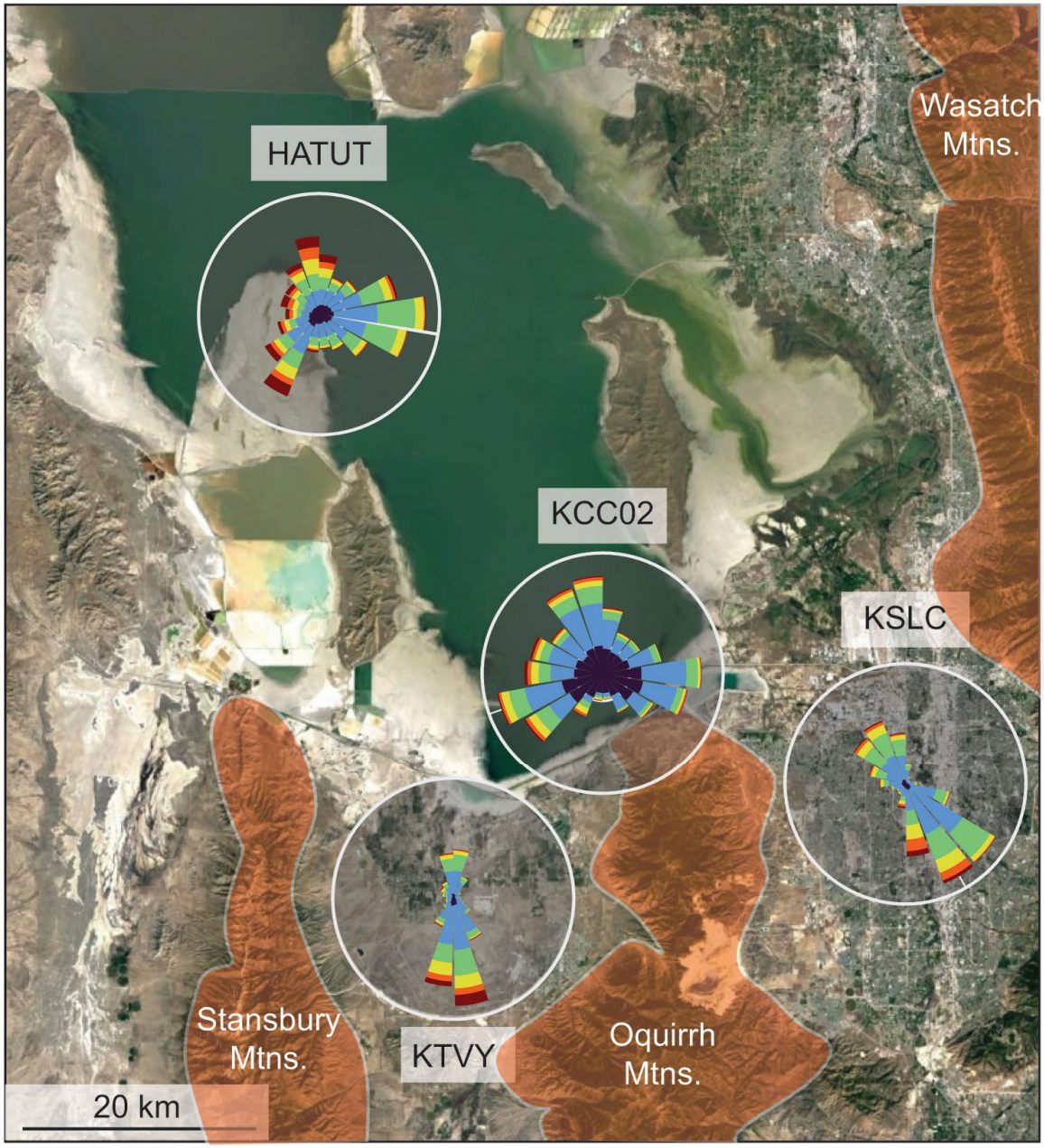

Figure 3. *Wind data for the study period from four stations in the MesoW est database. KTVY = Tooele Valley Airport, KSLC = Salt Lake City Airport, KCC02 = GSL State Park marina, HATUT = Hat Island.*

wave data, shear velocity is the most important variable for understanding sedimentary processes.

Unmanned Aerial Vehicle Photography

Ever since Eardley (1938) produced the first map of sediments in GSL, sedimentary studies in GSL have used multi-scale mapping to characterize shallow-water features such as bedforms and microbialites (Bouton and others, 2016a, 2016b; Vanden Berg, 2019; Smith and others, 2020; Baskin and others, 2021). Orthomosaic photos from unmanned aerial vehicles (UAVs) provide intermediate-scale maps that bridge field observations and satellite imagery. To facilitate comparisons with directional wave data, an orthomosaic was collected on June 29, 2022, from the Black Rock area using a DJI Mavic Air 2 at 200 ft standoff height via DroneLink mission planning software (Figure 1). A total of 877 orthophotos were collected and stitched together using PIX4Dcloud, covering an area of 0.278 km^2. Linear features within individual microbialites were measured using JmicroVision (Roduit, 2019) by tracing the long axes of 100 microbialite ridges from the mapped area as well as five lineations that crosscut the primary microbialite ridge orientation in the northwest corner of the mapped area.

Core Recovery and Grain Size Analysis

We collected three sediment cores using an SDI Vibecore Mini electric vibracore: one core from near Miera Spit (GSL22-MS) and two cores from near Black Rock (GSL22-BR-W and GSL22-BR-E) (Figure 1). We also collected an additional push core from a second location near Miera Spit (GSL22-SAI). We split each core using electric shears and collected ~15 mL sediment samples every 4 cm from one half of each core; the second half of each core was described and archived. Sediment samples were briefly rinsed with tap water to prevent grains from sticking together (due to salt precipitation from evaporating pore fluids) without dissolving minerals, then air dried. Grain size and shape of each sediment sample was analyzed using a Retsch Camsizer P4. Cores and subsamples of cores for analysis were registered with IGSNs (International Geo Sample Numbers) in the SESAR (System for Earth Sample Registration) database; parent core IGSNs are listed in the results section and subsamples from each core have unique IGSNs associated with their respective parent IGSN.

RESULTS

Observed Wind and Wave Conditions Near Black Rock and Miera Spit

Wind data over the study period were variable across MesoWest stations near Black Rock. South of Black Rock, wind stations have a predominantly N/S orientation. Data from Salt Lake City airport (station KSLC) are predominantly NW/SE while data from Bolinder-Tooele Valley Airport (station KTVY) are N/S. Wind orientations at both stations are consistent with previously observed lake breezes due to diurnal heating/cooling of the lake and land, as well as funneling of winds through the Salt Lake and Tooele Valleys, respectively (Ludwig and others, 2004). The station closest to Black Rock, KCC02, has strong N, E, and SW components. The near absence of strong and/or frequent winds from the south likely reflects obstruction from the nearby Oquirrh Mountains.

Overlapping time series of both wind and wave data suggested that wave orientations generally aligned with local wind orientations. Near Black Rock, wave observations, especially those with heights >15 cm, were oriented N/NNW (Figure 4). Less frequently, strong winds from the WSW produced waves arriving from this direction, most notably during late December of 2021 through early January 2022. Although wind data had multi-modal orientation, the rose diagram of wave directions had a strong modal peak oriented at 350°. In turn, the modal peak aligned with the long direction of the lake relative to the local shoreline. The largest wave heights were also observed in this direction, which was consistent with previous assumptions about fetch-limited wave conditions. In contrast, wave data from Miera Spit differed from those at Black Rock, even though they were collected over a relatively short interval (Figure 5). Significant wave events at Miera Spit were aligned with winds from the SW rather than the N/NNW.

Model-data Comparison for Black Rock

For model-data comparisons at Black Rock, we restricted our analysis to observations for which both wind and wave directions had an orientation of 350° +/- 10° based on the mode in wave directions (Figure 4). The estimated significant wave heights, peak wave periods, and shear velocities (red curves in Figure 6) were calculated as functions of wind speed along a fetch of 54 kilometers using Eqns. 1-7. Results show that the model slightly overestimates significant wave heights, and the effect is most pronounced at high wind speeds (Figure 6A). In contrast, model predictions for peak wave periods fall within the data (Figure 6B), although a normal Q-Q plot (Figure 6D) shows that the residuals are not normally distributed about the fit. Shear velocities predicted by model results also agree with those calculated with observed wave parameters (Figure 6C), although another Q-Q plot also shows some structure in the residuals (Figure 6F). No model-data comparison was performed for Miera Spit due to the shorter time interval and fewer wave measurements.

Core Sedimentology

Maximum depths of each core were 24 cm (GSL22-SAI; IGSN: 10.58052/IEEJT008B), 60 cm (GSL22-MS; IGSN: 10.58052/IEEJT008A), 77 cm (GSL22-BR-W; IGSN: 10.58052/IEEJT008C), and 74 cm (GSL22-BR-E; IGSN: 10.58052/IEEJT008D). For all cores, the maximum depth of coring represents the depth of a resistant hardground that we could not penetrate with our equipment. Sediments in cores from near Miera Spit (GSL22-MS and GSL22-SAI) were mainly composed of ooids with minor peloids (primarily *Artemia* fecal pellets), grapestones, and mica flakes; both cores lacked carbonate mud (Figure 7). Below 23 cm depth, ooid sands in the GSL22-MS core were roughly bimodal mixtures of fine and coarse ooids. Sediments in cores from near Black

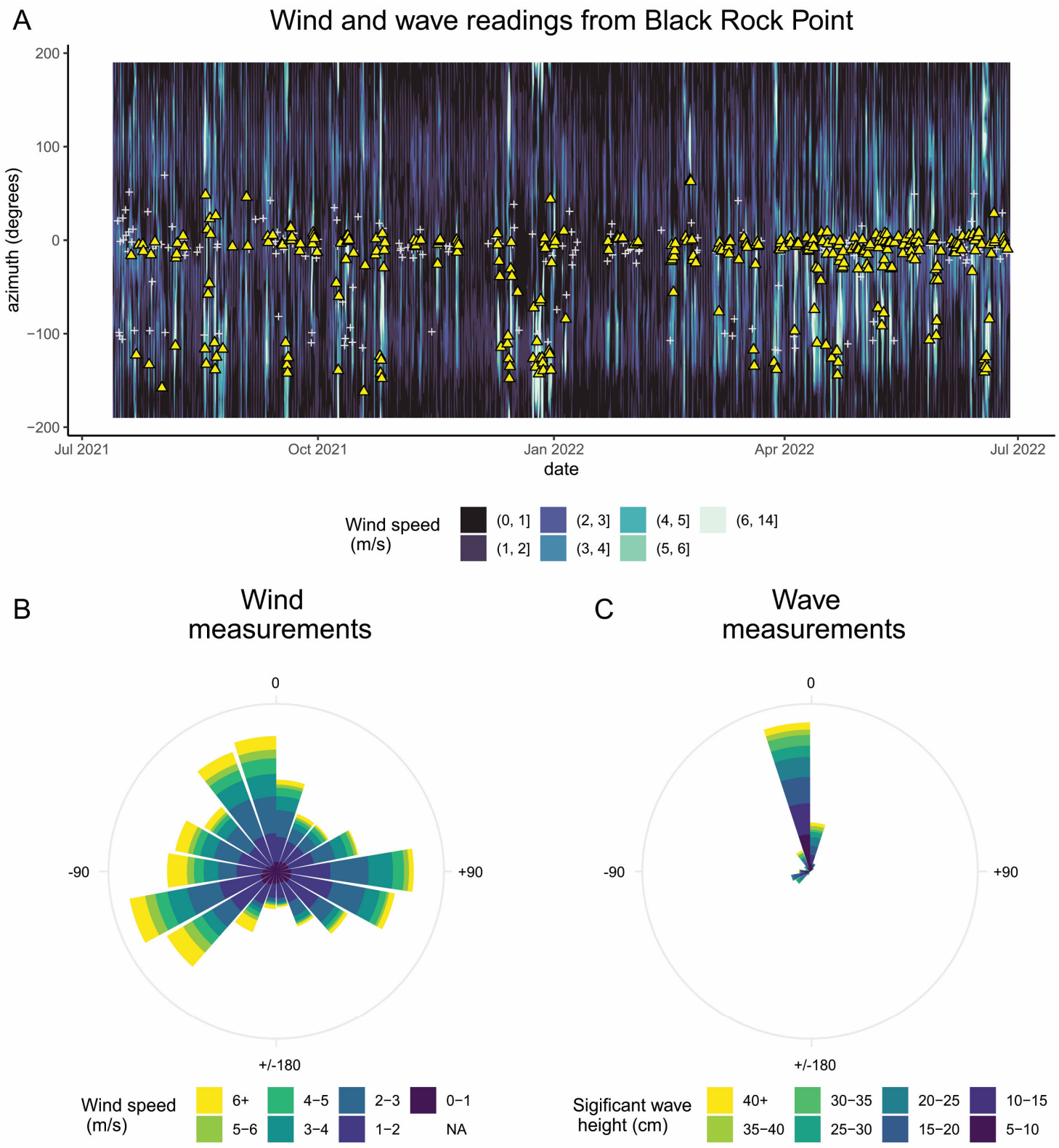

Figure 4. *Wind and wave observations near Black Rock collected from July 2021 to June 2022. A) Time series of wind speeds from a nearby wind station (KCCO2) plotted with significant wave heights from buoy #1356. The heatmap, which depicts wind speed and azimuth, shows that large wind events (light colors) are predominantly oriented N/NE with a secondary SW orientation. Significant wave heights >15 cm (yellow triangles) coincide with the timing and orientation of strong winds while wave heights <15 cm (grey crosses) have more variable orientations B) Rose diagram of wind measurements binned by 20° increments. Measurements are multimodal with W, S, and E peaks. C) Wave azimuths for significant wave heights. Wave directions were largely unimodal with an azimuth of 350° +/- 10°. Note that the dominant wave direction is both a frequent wind direction and a long fetch relative to the shoreline at Black Rock.*

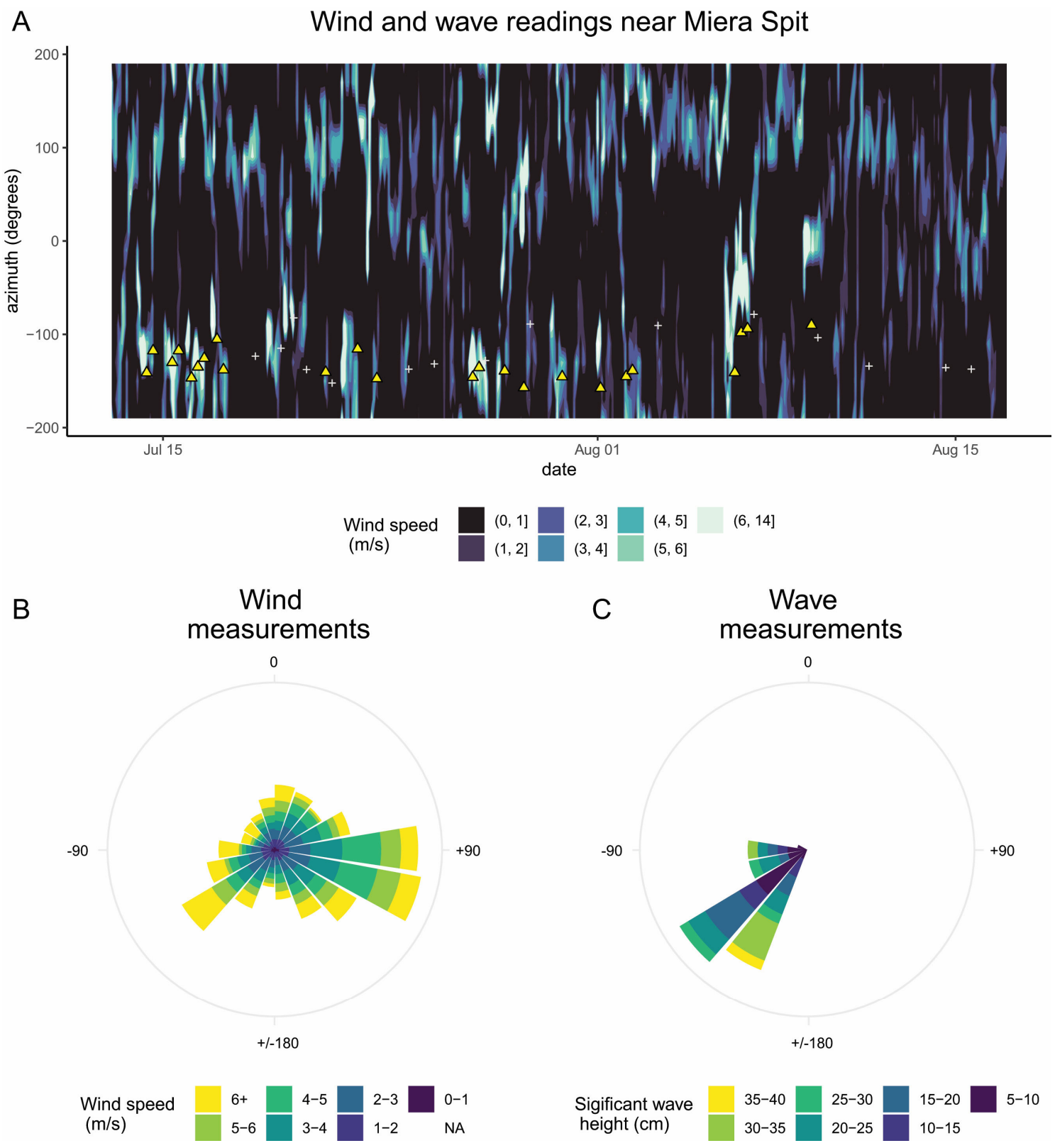

Figure 5. *Wind and wave observations near Miera Spit collected from July to August 2021. A) Time series of wind speeds from a nearby wind station (HATUT) plotted with significant wave heights from buoy #1328. The heatmap, which depicts wind speed and azimuth, shows that large wind events (light colors) are predominantly oriented E or SW. Significant wave heights >15 cm (yellow triangles) somewhat coincide with the timing and orientation of strong winds, although the match is weaker than at Black Rock. Wave heights <15 cm (grey crosses) have variable orientations. B) Rose diagram of wind measurements binned by 20° increments. Measurements are mostly bimodal with E and SW peaks. C) Wave azimuths for significant wave heights. Wave directions were largely unimodal with an azimuth of 210° +/- 10°. Note that the dominant wave direction differs from Black Rock (Figure 4), reflecting differences between wind and shoreline orientation between the two sites.*

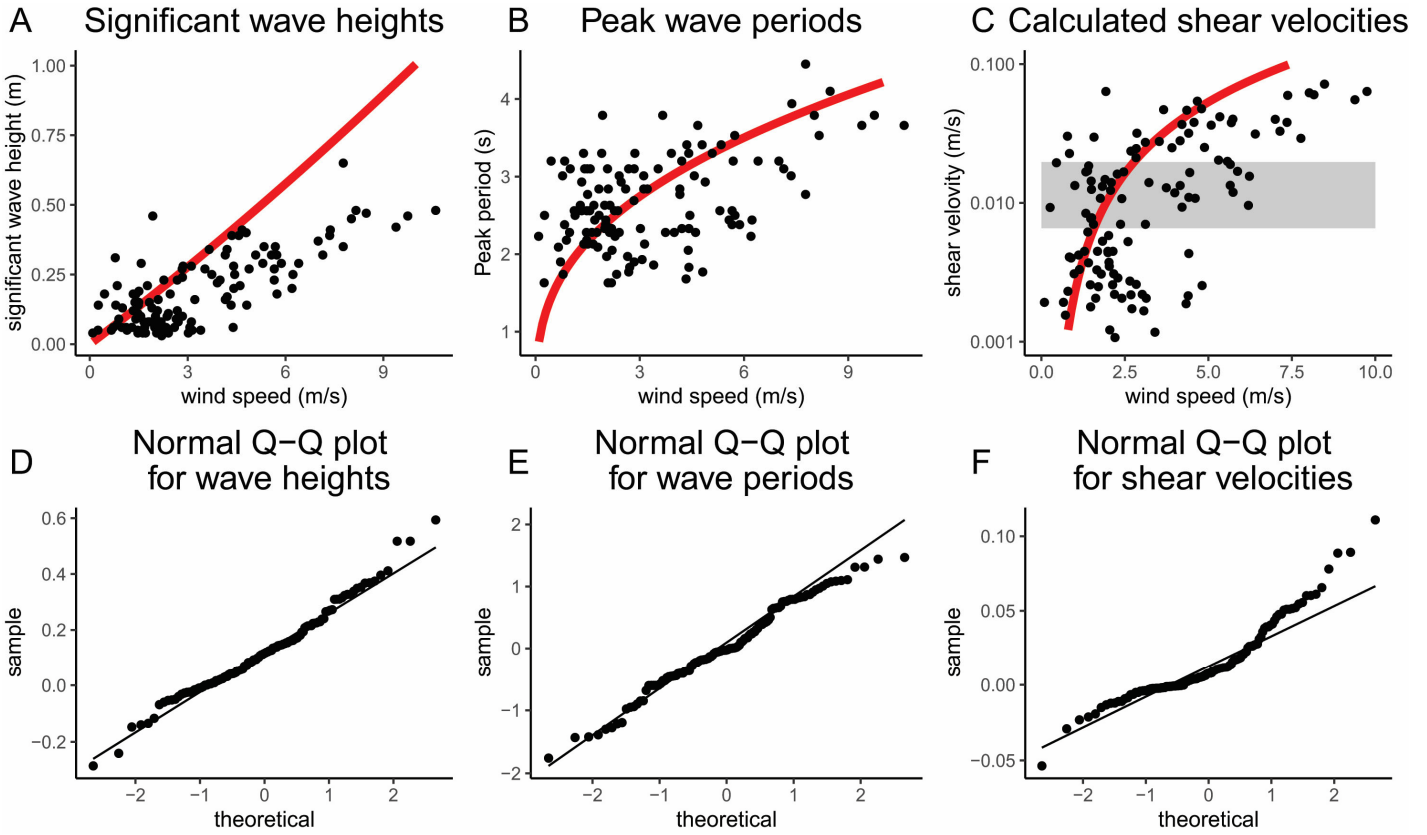

Figure 6. *Comparison of wind speed with significant wave heights (A), peak periods (B), and calculated shear velocities (C). Black circles represent simultaneous measurements of wind speed from station KCC02 matched with wave measurements at buoy #1356. Points represent a subset of wind and wave measurements with an azimuth of 350° +/- 10°. For A and B, red curves show wave parameters (vertical axes) as a function of wind speed as calculated by Eqns. 1-7 with a constant fetch of 54 km. For C, shear velocities were calculated using Eqns. 8-10. Black circles show shear velocities calculated using buoy observations of wave height and peak periods, while the red curve uses wave heights and peak wave periods calculated from Eqns. 1-7. The shaded gray bar shows the range of shear velocities most relevant to sediment transport near Black Rock: the lower and upper bounds represent thresholds for motion and suspension, respectively, for 370 µm sand.*

Rock (GSL22-BR-W and GSL22-BR-E) were composed of dark green- to dark orange-brown-pigmented, gravel-sized microbial mat or partially mineralized microbialite fragments (referred to as "pustular grains" and "microbial popcorn" by Chidsey and others (2015), grapestones, angular carbonate sand grains (not ooids), and peloids (also primarily *Artemia* fecal pellets) (Figure 7); with the exception of a few horizons, both cores lacked muddy matrix. Both Black Rock cores shared a similar sequence of ~20 cm of gravel-sized microbial mat and microbialite fragments overlying 40-50 cm of grapestone-dominated sediment. Core GSL22-BR-E had an additional 10.5-cm-thick layer of fine ooid sand overlying the microbialite fragment layer. Grapestone compositions included aggregates of ooids, peloids, and microbialite fragments.

The grain size and shape data are distinctly different between the Miera Spit and Black Rock sediment cores (Figure 8). Median grain diameters (D_{50}) in the Miera Spit cores range from 369-496 µm (GSL22-MS) and 332-434 µm (GSL22-SAI), with mean roundness in both cores ranging from 0.71-0.77. These values are similar to previously characterized GSL ooids (Trower and others, 2020), although the GSL22-MS core includes D_{50} values that are greater than reported in other areas. The grain size and roundness trends with depth are very similar between the two Miera Spit cores, showing little variability, although ooids in the GSL22-MS core are consistently larger than those in the GSL22-SAI core. In comparison, the Black Rock cores depict more variability, where the two Black Rock cores differ most in the upper 20 cm. These trends match the lithologic variability observed in the cores (Figure 8): samples in the upper 10.5 cm of GSL22-BR-E have median grain diameters (D_{50} = 281-322 µm) and mean roundness (0.72-0.78) characteristic of ooids, while the microbial mat and microbialite fragments were very coarse sand to very fine gravel sized (D_{50} = 1448-3528 µm) and angular (mean roundness = 0.32-0.37) and the grapestones were coarse to very coarse sand sized (D_{50} = 911-1839 µm) and angular (mean roundness = 0.36-0.43). Grapestones in the GSL22-BR-W core were consistently coarser than the GSL22-BR-E core.

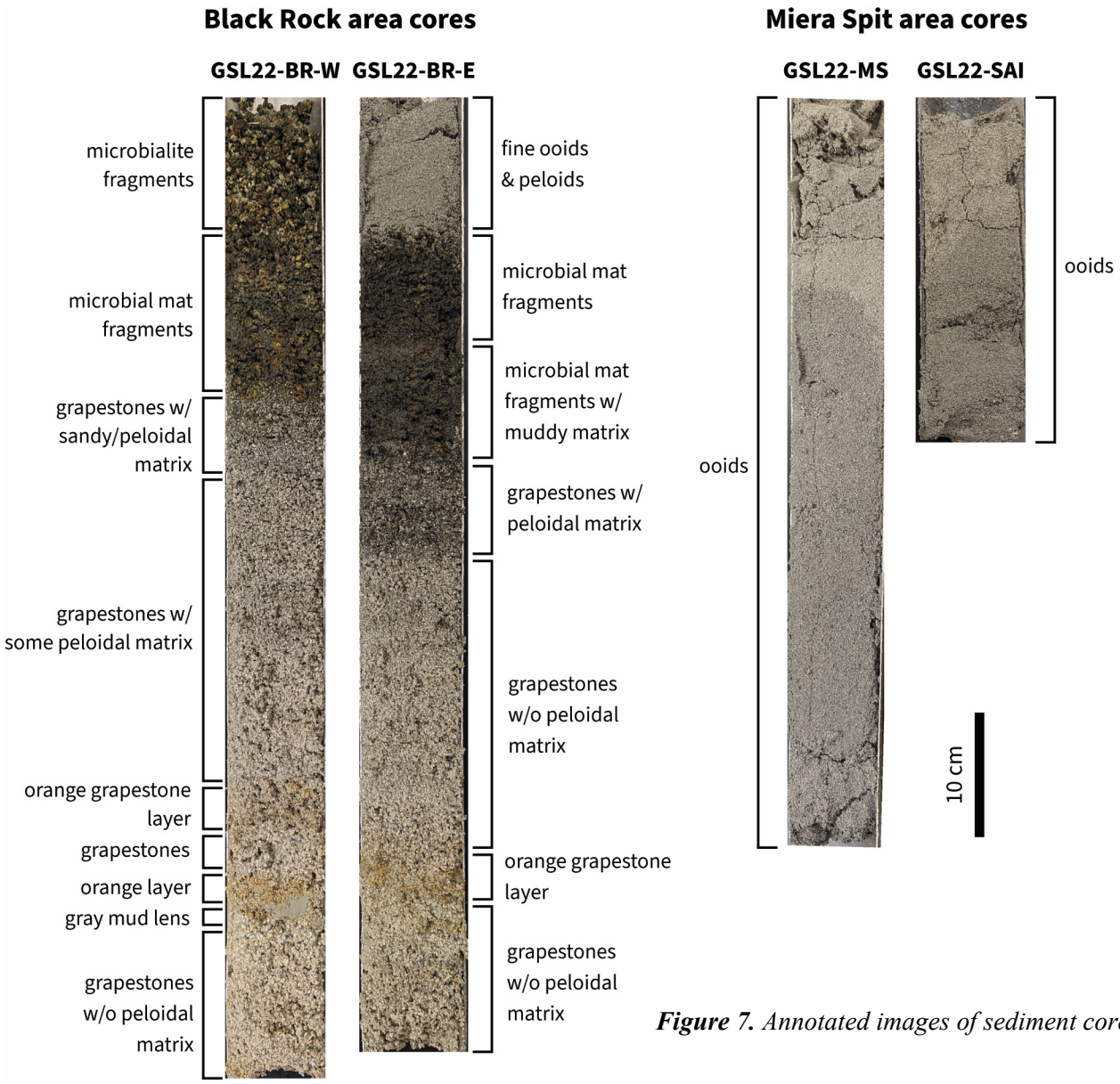

Figure 7. *Annotated images of sediment cores.*

Together, the core sedimentology data indicate that the Miera Spit area has historically been characterized almost exclusively by the production and deposition of ooid sand. In contrast, the Black Rock area was instead a grapestone factory prior to the more recent development of a continuous blanket of microbialites, overlain by a mobile and transient layer of ooid sand. Although the sets of Miera Spit and Black Rock cores were both significantly more similar amongst each set than between sets, both sets of cores displayed more subtle but systematic differences in grain size associated with their different locations along each shoreline.

UAV imagery of microbialite forms

UAV orthomosaic imagery at Black Rock reveals the orientations of exposed microbialite ridges (Figure 9). Individual microbialite ridges trend NNW/SSE along long axes. Multiple microbialites from the northwestern corner of the orthomosaic form an additional array of lineations roughly 20-25 m in length, trending NE/SW.

DISCUSSION

Wave Orientations Differ Between Sites

The differing wave orientations at the two sites reflect differences in the fetch between the two shorelines. At Black Rock, the predominant N/NNE wave orientation aligns with the long direction of the lake, and thus the longest available fetches. At a broader level, the regional geology provides an underlying factor linking basin orientation and diurnal wind patterns. Both the shape of the lake and the NNE/SSE wind directions follow the strong topography of nearby mountain ranges such as the Wasatch in the east

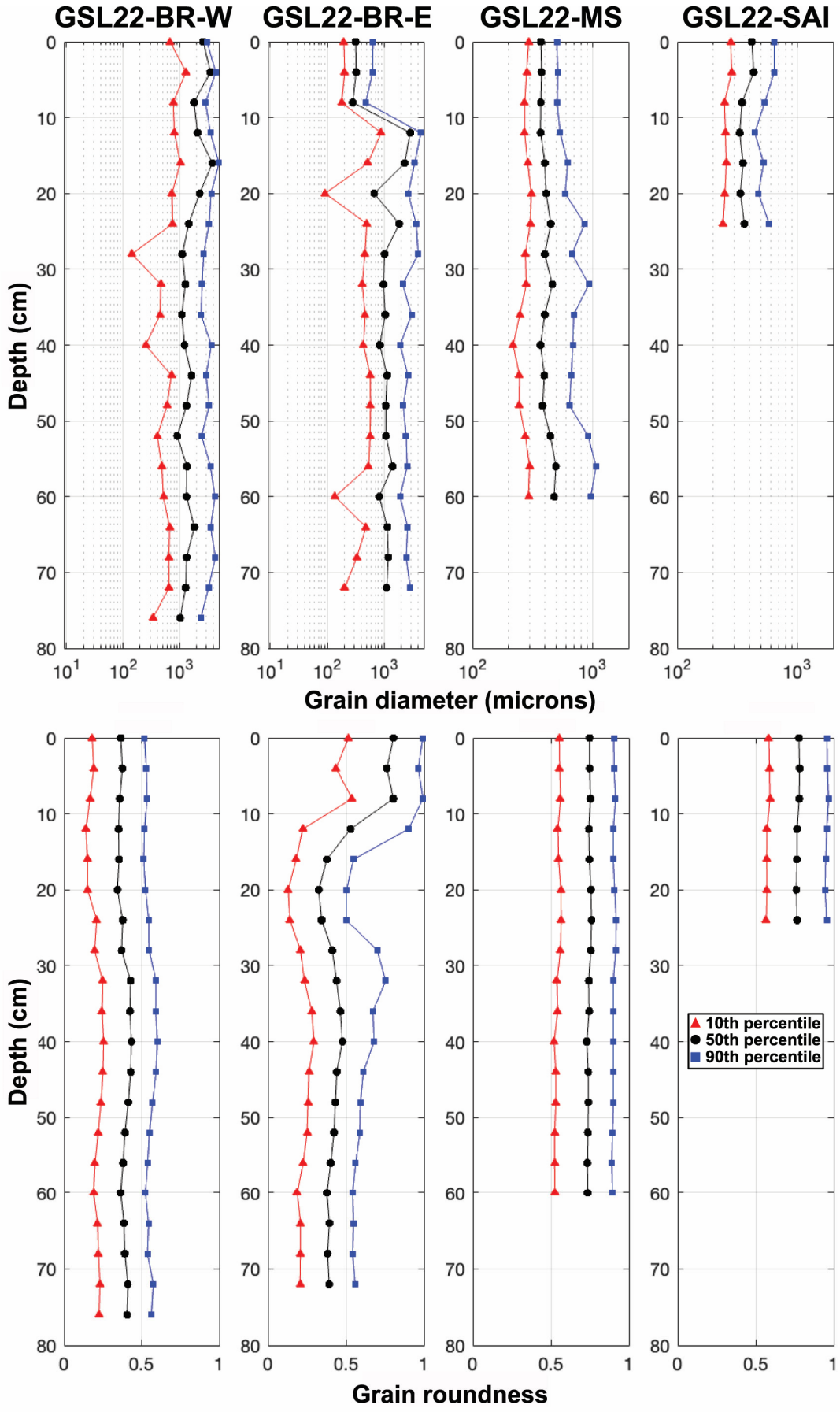

Figure 8. *Grain diameter and roundness from the four collected cores. Diameter and roundness metrics derived from Camsizer output data, where the red line indicates the 10th percentile (triangles), black indicates the 50th percentile (circles), and blue indicates the 90th percentile (squares).*

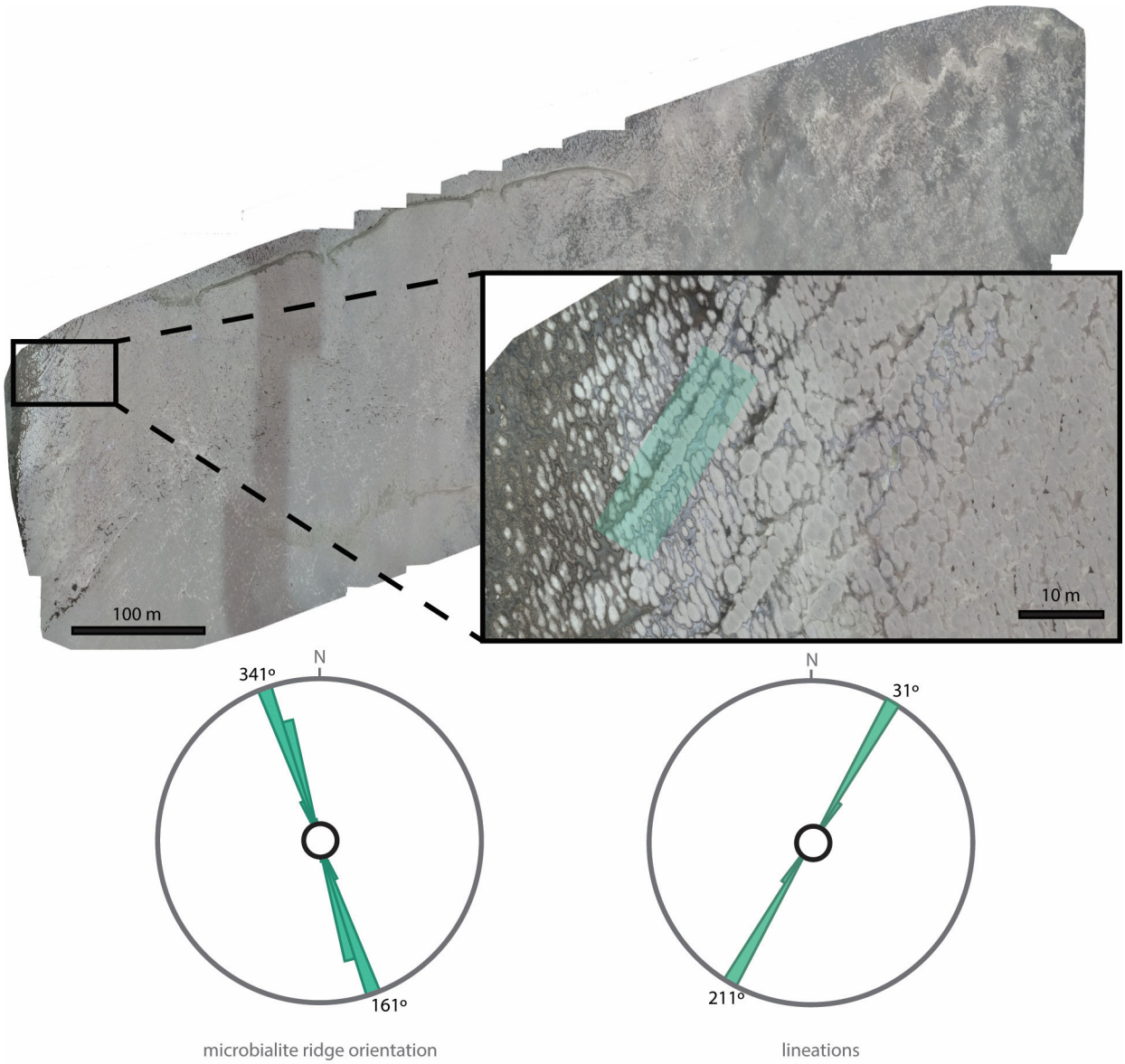

Figure 9. *UAV image of exposed microbialite ridges west of Black Rock, near buoy #1356. Individual microbialite ridges trend NNW/SSE along long axes. Multiple individual microbialite ridges group together to form arrays of lineations that trend NE/SW, highlighted in teal in image inset.*

(Figure 3). These effects are especially strong towards the south end of the lake where onshore/offshore lake breezes are funneled through the Tooele and Salt Lake valleys (Figure 3). Although the windrose for the marina (KCC02) is more complex than those in the valleys, the nearly unimodal wave directions from the north can be explained by short fetches for winds not aligned to the north.

In contrast, wave orientations at Miera Spit have a different alignment because the shoreline is nearly perpendicular to its counterpart near Black Rock. Winds from the N/NNW have short fetches obstructed by Antelope Island, Gunnison Island, and Promontory Point. Instead, most waves had a SW orientation, which is consistent with the analysis of nearby wave ripples and bar forms by Smith and others (2020). The regional wind patterns that generate these waves differ from the predominant NNW/SSE winds along the basin axis, but are aligned with the predominant southwesterly to southeasterly orientation of the strongest winds in the eastern and southern Bonneville basin from 1946–1993 compiled by Jewell (2007).

Waves, Microbialite Morphologies, and Paleoflow Indicators

At first glance, the near-unimodal orientation of waves at Black Rock provides a compelling test of microbialite ridge orientations as paleoflow indicators. However, even a first-order analysis precludes a 1:1 mapping of microbialite ridge orientation onto wave directions. First, there are at least two sets of su-

perimposed linear microbialite orientations in the area we analyzed near the Black Rock buoy, and the expected orientation of either set of linear features relative to the dominant wave direction likely depends on their origin. For example, Vanden Berg (2019) documented incipient microbialites forming on the crests of wave ripples. If some lineations in mature microbialites reflect underlying nucleation on bedforms, then the lineations should be perpendicular to the direction of the waves. In contrast, the long axes of microbialite ridges near the Black Rock buoy have a strong onshore/offshore orientation that is nearly parallel to measured wave directions. Thus, even when wave orientation reasonably influences microbialites, the orientation of lineations relative to wave features–and thus, their use as a paleoflow proxy–is complex. Additionally, other origins for strong lineations (e.g., underlying faults and fractures) must be accounted for.

A more complete understanding of potential paleoflow indicators has several spatial and temporal correlations. For example, why are the onshore-offshore lineations at Black Rock rotated with respect to measured wave orientations? One possibility is that waves observed at the buoy refract as they interact with steep and irregular bathymetry near the shoreline. Another possibility is that microbialites reflect a time-integrated signal of wave conditions, and that direct comparison to modern waves represents a recency bias. Addressing this issue requires more data on the absolute ages of microbialites and their underlying sediments from the vibracore recoveries (Figure 7). Sediments from Miera Spit and the Black Rock shoreline have not been previously dated with radiocarbon. However, radiocarbon dating of microbialites from the northern shores of Antelope Island (i.e., Bridger Bay, Buffalo Point, and White Rock Bay) and from the North Arm have suggested at least two pulses of microbialite formation from ~11.4 and 8 ka, and 3.8 and 1.7 ka (Bouton and others, 2016b; Newell and others, 2017, 2020). Furthermore, radiocarbon dating of GSL ooids from northern Antelope Island (Bridger Bay) and the North Arm (Spiral Jetty) suggest that ooids at the modern sediment surface have been slowly accumulating over the past ~6 ka (Paradis, 2019). Together, these data suggest that the microbialites on the Black Rock shoreline are likely at least 1.7 ka in age, and potentially thousands of years older. A dominant NNW orientation may therefore reflect basin orientation and tectonic effects on topography, which are stable over these time periods. The deviation from modern waves could be also explained by differences in wind patterns due to variations in Holocene climate, as well as differences in lake level and surface area. Nevertheless, because the Rohweder and others (2008) wave model performs relatively well at matching the modern wave data, we suggest that this model could be a useful tool to evaluate how different wind patterns and/or lake level in the past might better explain the microbialite ridge orientations.

Influences of Wave-driven Sediment Transport on Sedimentary Facies

Two notable sedimentological differences between the Miera Spit and Black Rock sites could be related to differences in transport mode and frequency: (1) the relatively large ooid diameters at Miera Spit (primarily upper medium sand sized, whereas most ooids elsewhere in the lake including at Black Rock are lower medium sand sized); and (2) the contrast between ooid-dominated sediments at Miera Spit and grapestone-dominated sediments (at depth in cores) at Black Rock. Here, we suggest hypotheses about how transport mode and frequency may influence the distinct sedimentology of these sites and use our data to provide an initial evaluation of these hypotheses.

Trower and others (2020) noted that the aragonite saturation state (Ω_{Ar}) of GSL water is lower than that characteristic of seawater in modern marine ooid-forming environments. This relatively low Ω_{Ar} value explains the relatively small sizes of GSL ooids because it results in relatively slow precipitation rates and therefore smaller equilibrium ooid sizes (Trower and others, 2017). Furthermore, GSL ooids are so small due to low lake water Ω_{Ar} that many of their sizes are close to the threshold below which impacts are completely viscously damped, resulting in no abrasion. Due to this effect, increasingly frequent transport events (i.e., increasing intermittency, f_{int}) cannot reduce ooid size beyond ~200 μm. Many GSL ooid sizes are close to this threshold (Figure 10). However, Miera Spit is unique in that ooids there have grown to larger sizes than observed in other locations. Within the equilibrium ooid size framework, we would therefore predict that the larger ooid sizes at Miera Spit must be associated with either less frequent transport (lower f_{int}), or more energetic transport (higher u_*) (Figure 10). Model-based estimates of intermittency of movement suggest similar values in the range of 1-2% (f_{int} = 0.01 - 0.02) at these two sites (Smith and others, 2020; Trower and others, 2020). Due to the limited size of the Miera Spit dataset, we are unable to make a robust comparison of shear velocities at the two sites to assess whether differences in u_* might be driving the larger ooid sizes at Miera Spit. An analysis of wind patterns along the eastern and southern margins of the Bonneville basin over a

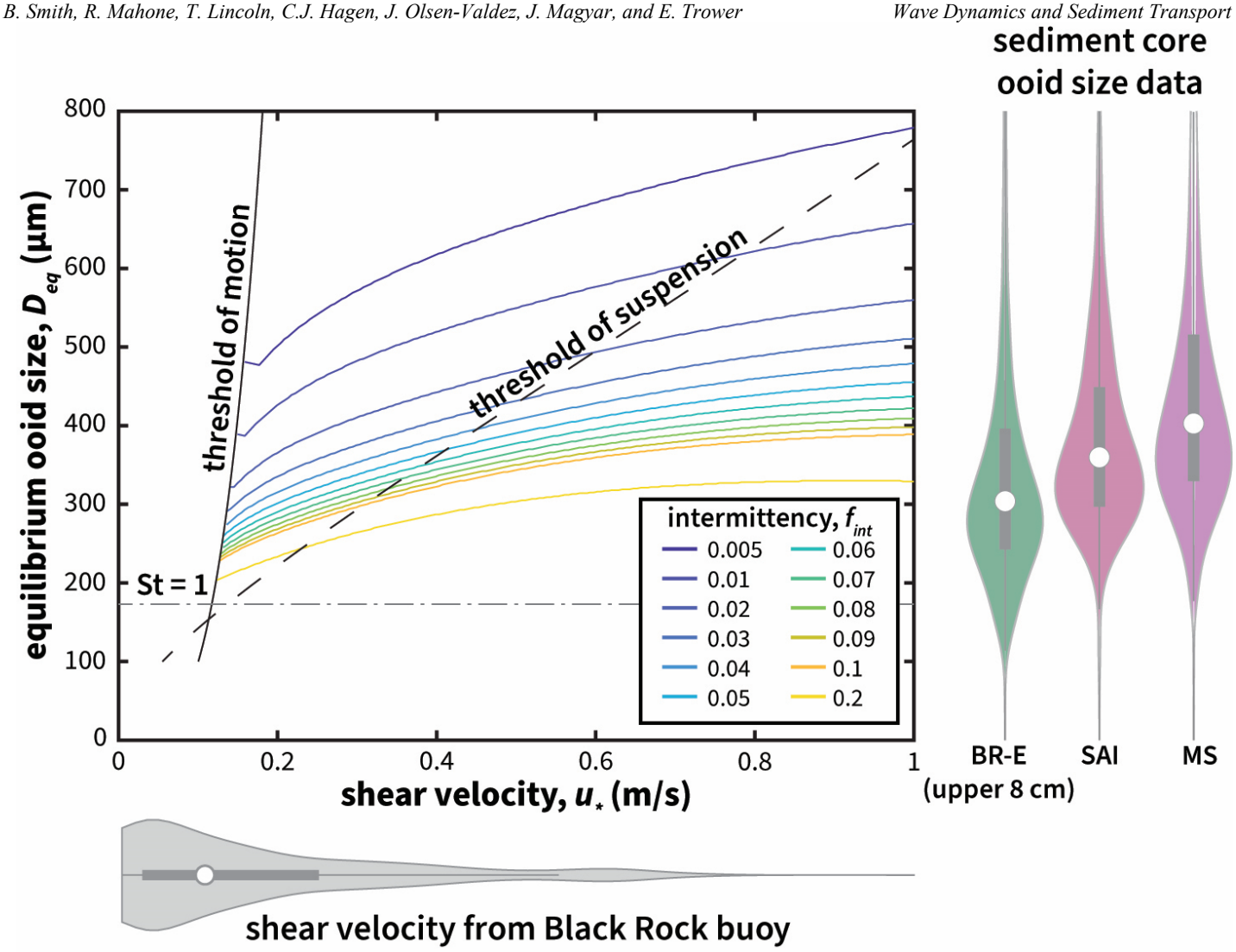

Figure 10. Plot of predicted equilibrium ooid sizes (D_{eq}) as a function of bed shear velocity (u_*) following Trower and others (2017) for a range of intermittencies (f_{int}), compared with violin plots of shear velocities from the Black Rock buoy (horizontal violin) and pooled ooid size data from the three cores that contained ooid-dominated layers (vertical violins). Solid black line shows threshold of motion, dashed black line shows threshold of suspension, and the dash-dot black line shows the viscous damping threshold (Stokes number, St = 1) below which grains cannot abrade. The larger ooids at Miera Spit could be explained by lower intermittency (less frequent transport) and/or higher shear velocity.

longer observation duration than our study indicated that the strongest modern winds were from the SW-SE over the period between 1946–1993 (Jewell, 2007). These southwesterly to southeasterly winds would have resulted in higher shear velocities at Miera Spit than at Black Rock due to the differences in fetch.

The dynamics of grapestone formation have been less thoroughly examined than those of ooids. Some workers have suggested that microbially-mediated carbonate mineral precipitation plays a key role in grapestone formation (Purdy, 1963; Winland and Matthews, 1974; Fabricius, 1977; Diaz and others, 2022). If this process is the key factor driving the formation of grapestones in GSL, we might expect to see microbial community differences between the Miera Spit and Black Rock areas. Although we did not collect microbial diversity data as part of this study, Ingalls and others (2020) did report some notable differences between ooid-dominated sediments from Bridger Bay (on the northern part of Antelope Island) and ooid-dominated sediments between Black Rock and GSL State Park. In particular, relative to samples from the GSL State Park/Black Rock site, samples from Bridger Bay lacked cyanobacteria (which are commonly implicated in driving carbonate precipitation) and had more abundant *Chloroflexi* and *Deinococcus-Thermus* sequences (Ingalls and others, 2020). However, there is no evidence directly linking this specific microbial community difference to sedimentary facies differences between those two sites. Further microbial community analyses of the Miera Spit area might help to better evaluate this hypothesis. However, it is not clear that the modern surface microbial community at each site would be representative of the community that was present when sediments at the base of each core were forming, particularly given that the modern lake microbial community

has already been influenced by the recent historically low lake levels (Frantz and others, 2022).

Alternatively, one could also speculate that physical, rather than biological, processes are responsible for the Black Rock grapestone factory. Grapestone formation is commonly thought to reflect very infrequent but very energetic transport, providing long rest periods for grains to be cemented together with transport events that can still entrain these relatively coarse compound grains. This explanation appears to conflict with the relatively similar estimates of intermittency between the two sites and our interpretation of higher shear velocities at Miera Spit based on differences in ooid size. The grapestones in the Black Rock cores could therefore reflect an older and deeper lake stage than that represented by ooids in either location. This idea is supported by our observation of grapestones in surface sediments (collected via dredge), which we only found in deeper waters (2.5-3 m water depth) off the southern Antelope Island shoreline (Figure 11). There, grapestones occurred in the troughs between microbialite mounds and ooids were rare. In contrast, we did not find any grapestones in microbialite troughs near Black Rock, suggesting that, currently, transport conditions are not as conducive to grapestone formation even in deeper

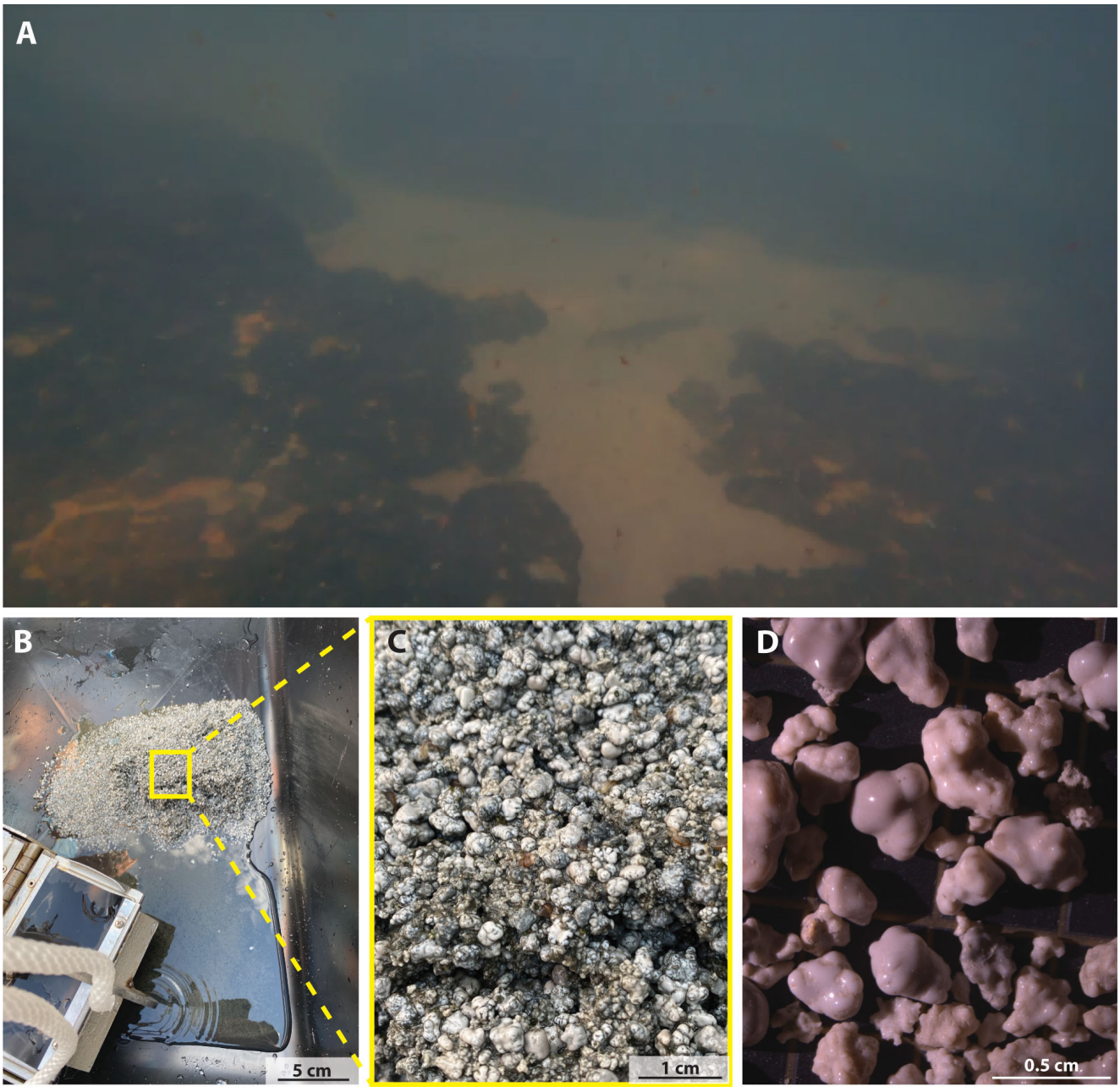

Figure 11. *Images of grapestones collected by dredge at the modern sediment surface in deeper water near the southern tip of Antelope Island. A) Grapestones occurred in patches of mobile sediment in troughs between microbialites, as illustrated in this image from a submersible remotely-operated vehicle (ROV). B-C) Grapestone-rich sediment collected by dredge (B) and zoomed-in field image of grapestone-rich sediment (C). D) Stereoscope image of grapestones from this location.*

water along that shoreline. Morphological analyses of spits associated with older Bonneville shorelines suggest that in the late Pleistocene (i.e., prior to the Gilbert episode (Oviatt, 2014)), wave transport in the lake was dominated by strong northerly to northwesterly storms (Schofield and others, 2004; Jewell, 2007). Infrequent but strong wave currents from these types of storms could be consistent with the optimal shoreline orientation and location for grapestone development in the past differing from that in the modern lake. Geochronological constraints and petrographic analysis of buried grapestone sediments at Black Rock are needed to further test this hypothesis and evaluate the roles of microbial community versus hydrodynamics on grapestone formation in GSL. Again, given the relatively good fit between the Rohweder and others (2008) model and the wave buoy data for the Black Rock area, we suggest that the model would be a useful tool to reconstruct historical wave conditions in this area.

Strengths, Weaknesses, and Potential Applications of Model

Cross-validation of wave models with buoy data provides several key takeaways for future studies of GSL across past, present, and future. In optimal cases (i.e., when high-quality, continuous wind data are available near the shoreline of interest), fetch-limited wave models yield reasonable results for key variables such as shear velocities. However, the plots of the residuals in Figures 6D-F suggest that there is unexplained structure in wave observations that are not captured by the model. A likely source of discrepancies is that some of the empirical constants in Eqns. 1 -7 were calibrated for seawater, which is less dense than GSL lake water. In particular, the drag coefficient in Eqn. 1 is sensitive to temperature and density variations of both air and water (Le Roux, 2009). A density effect could reasonably affect all three parameters in Figures 6A-C since they all involve the drag coefficient. Le Roux (2009) also notes that fluids denser than seawater—for example, those with high suspended sediment loads—produce waves that are smaller than those predicted by Eqns. 1-7. The overprediction of wave heights observed in Fig. 6A is thus consistent with a density effect.

The dependence on nearby wind stations is both a challenge and an opportunity. Even with limited results from Miera Spit and Black Rock, fetch-based wave models reasonably predict spatial differences in shear velocities and frequencies of motion that are crucial for further studies of how sedimentary facies are distributed across GSL. However, the variety of wind conditions observed at different MesoWest stations (Figure 3) strongly suggests that the quality of modeled wave parameters strongly depends on the proximity of relevant wind data. For example, onshore data from Salt Lake City (KSLC) and Tooele-Bolinder Airport differ considerably from stations on the shores of the lake itself, such as KCC02 and HATUT. At a more granular level, predicting conditions along specific shorelines requires local wind data. At present, the marina has two wind stations relevant to GSL State Park (AS768 and KCC02), but relevant wind data for Antelope Island State Park have been challenging to obtain since the loss of the Bridger Bay station in 2018. While data from other stations, such as Hat Island (HATUT), may be appropriate for sedimentary research, more proximal data is needed should these wave models become important for GSL conservation efforts and policymaking (Rohweder and others, 2008).

Even a rudimentary agreement between wave models and empirical data opens the door to using these models to study how past anthropogenic and climatic changes may have modulated the sedimentary facies we observe today. For example, construction of the causeway divided the lake into chemically distinct North and South Arms; did this causeway also change effective fetches, especially for shorelines near Black Rock? Since the causeway is recent within the context of the lake's Holocene inception, modeling pre-causeway conditions might prove instructive for interpreting both surficial and cored sediment data collected from near GSL State Park (Figure 7). For natural climatic variations, previous research has suggested that Lake Bonneville and other paleolake shorelines were associated not only with higher lake levels, but different prevailing winds (Schofield and others, 2004; Jewell, 2007). While linkages between lake level, paleoclimate, and lake chemistry strongly affect carbonate facies, fetch-limited wave models may provide a more holistic view of how paleolake levels related to sediment transport conditions beyond simple changes in water depth.

Finally, it is worth noting that the fetch-limited wave models used here and in previous work (Smith and others, 2020; Trower and others, 2020) have applications outside of sedimentary geology, such as for environmental forecasting and conservation. In fact, the Arc plugin used in these studies (Rohweder and others, 2008) was originally developed by the USGS for environmental conservation and management. While environmental forecasts and recommendations are beyond the scope of this work, we do point out that basic model-data comparisons–especially with respect to shear velocity and sediment mobility–are fundamental to future applications of lake modeling

with regards to GSL environmental conservation and policy making.

ACKNOWLEDGEMENTS

Permission to temporarily anchor buoys to the lakebed was granted by the State of Utah Department of Natural Resources under Right of Entry Permit No. 410-00698. Additional permission to access the lake shore at Miera Spit by land via Antelope Island State Park was provided by Utah Division of Parks and Recreation Special Use Permit P72-21.

REFERENCES

Abbott, B.W., Baxter, B.K., Busche, K., de Freitas, L., Frei, R., Gomez, T., et al., 2023, Emergency measures needed to rescue Great Salt Lake from ongoing collapse.

Baskin, R.L., and Allen, D.V., 2005, Bathymetric Map of the South Part of Great Salt Lake, Utah, 2005: USGS.

Baskin, R.L., and Turner, J., 2006, Bathymetric Map of the North Part of Great Salt Lake, Utah, 2006: USGS.

Baskin, R.L., Della Porta, G., and Wright, V.P., 2021, Characteristics and controls on the distribution of sublittoral microbial bioherms in Great Salt Lake, Utah: implications for understanding microbialite development: The Depositional Record, dep2.159, https://doi.org/10.1002/dep2.159

Beisner, K., Naftz, D.L., Johnson, W.P., and Diaz, X., 2009, Selenium and trace element mobility affected by periodic displacement of stratification in the Great Salt Lake, Utah: The Science of the Total Environment, 407(19), 5263–5273.

Belovsky, G.E., Stephens, D., Perschon, C., Birdsey, P., Paul, D., Naftz, D., et al., 2011, The Great Salt Lake Ecosystem (Utah, USA): long term data and a structural equation approach: Ecosphere, 2(3), art33.

Bouton, A., Vennin, E., Boulle, J., Pace, A., Bourillot, R., Thomazo, C., et al., 2016a, Linking the distribution of microbial deposits from the Great Salt Lake (Utah, USA) to tectonic and climatic processes: Biogeosciences, 13(19), 5511–5526.

Bouton, A., Vennin, E., Mulder, T., Pace, A., Bourillot, R., Thomazo, C., et al., 2016b, Enhanced development of lacustrine microbialites on gravity flow deposits, Great Salt Lake, Utah, USA: Sedimentary Geology, 341, 1–12.

Carozzi, A.V., 1962, Observations on Algal Biostromes in the Great Salt Lake, Utah: The Journal of Geology, 70(2), 246–252.

Chidsey, T.C., Vanden Berg, M.D., and Eby, D.E., 2015, Petrography and characterization of microbial carbonates and associated facies from modern Great Salt Lake and Uinta Basin's Eocene Green River Formation in Utah, USA: *In* Bosence, D.W.J., Gibbons, K.A., Heron, D.P.L, Morgan, W.A., Pritchard, T., and Vining, B.A. (eds.), Microbial Carbonates in Space and Time: Implications for Global Exploration and Production, London: The Geological Society of London. Vol. 418, 261–286.

Coastal Engineering Research Center, 1984, Shore Protection Manual. US Army Corps of Engineers. https://doi.org/10.5962/bhl.title.47829

Collins, N., 1980, Population ecology of Ephydra cinerea Jones (Diptera: Ephydridae), the only benthic metazoan of the Great Salt Lake, U.S.A: Hydrobiologia, 68(2), 99–112.

Colman, S.M., Kelts, K.R., and Dinter, D.A., 2002, Depositional history and neotectonics in Great Salt Lake, Utah, from high-resolution seismic stratigraphy: Sedimentary Geology, 148(1), 61–78.

Diaz, M.R., Eberli, G.P., and Weger, R.J., 2022, Indigenous microbial communities as catalysts for early marine cements: An in vitro study: The Depositional Record. https://doi.org/10.1002/dep2.202

Eardley, A.J., 1938, Sediments of Great Salt Lake, Utah: AAPG Bulletin, 22(10), 1305–1411.

Fabricius, F.H., 1977, Origin of marine oöids and grapestones. *In* Fuchtbauer, H., Lisitzyn, A. P., Milliman, J. D., and Seibold, E. (Eds.), Vol. 7, Schweizerbart.

Frantz, C., Gibby, C., Nilson, R., Aeschlimann, J., Athalye, R., Christensen, C., et al., 2022, Documenting a geobiological tragedy: The exposure of Great Salt Lake's microbialites and the undergraduate researchers at the vanguard: GSA Connects 2022, Denver, CO.

Homewood, P., Mettraux, M., Vanden Berg, M.D., Foubert, A., Neumann, R., Newell, D., and Atwood, G., 2022, Onshore groundwater spring carbonate mounds to lacustrine microbialites, the perplexing record of a transitional Great Salt Lake carbonate shoreline at Lakeside, Utah: The Depositional Record, 8(1), 9–38.

Horel, J., Splitt, M., Dunn, L., Pechmann, J., White, B., Ciliberti, C., et al., 2002, Mesowest: Cooperative Mesonets in the Western United States: Bulletin of the American Meteorological Society, 83 (2), 211–226.

Ingalls, M., Frantz, C.M., Snell, K.E., & Trower, E.J., 2020, Carbonate facies-specific stable isotope data record climate, hydrology, and microbial communities in Great Salt Lake, UT: Geobiology, 18

(5), 566–593.
Jewell, P.W., 2007, Morphology and paleoclimatic significance of Pleistocene Lake Bonneville spits: Quaternary Research, 68(3), 421–430.
Jones, E.F., and Wurtsbaugh, W.A., 2014, The Great Salt Lake's monimolimnion and its importance for mercury bioaccumulation in brine shrimp (*Artemia franciscana*): Limnology and Oceanography, 59(1), 141–155.
Le Roux, J.P., 2009, Characteristics of developing waves as a function of atmospheric conditions, water properties, fetch and duration: Coastal Engineering, 56(4), 479-483.
Ludwig, F.L., Horel, J., and Whiteman, C.D., 2004, Using EOF Analysis to Identify Important Surface Wind Patterns in Mountain Valleys: Journal of Applied Meteorology, 43(7), 969–983.
Mahon, R.C., Trower, E.J., Smith, B.P., Lincoln, T.A., Olsen-Valdez, J., Magyar, J.S., and Hagen, C.J., 2023, 2D Wave Spectral Data, South Arm, Great Salt Lake, Utah: DOI: https://doi.org/10.46428/sld
Newell, D.L., Jensen, J.L., Frantz, C.M., and Vanden Berg, M.D., 2017, Great Salt Lake (Utah) microbialite δ13 C, δ18 O, and δ15 N record fluctuations in lake biogeochemistry since the late Pleistocene: Geochemistry, Geophysics, Geosystems, 18(10), 3631–3645.
Newell, D.L., Vanden Berg, M.D., Fernandez, D.P., Frantz, C.M., and Jensen, J.L., 2020, Radiocarbon and u-Th double-dating and isotope geochemistry of great Salt Lake microbialites: Implications for the 14c reservoir and paleolake biogeochemical evolution: 72nd Annual GSA Rocky Mountain Section Meeting, Geological Society of America. https://doi.org/10.1130/abs/2020rm-346645
Oviatt, C.G., 2014, The Gilbert Episode in the Great Salt Lake Basin, Utah: Miscellaneous Publication 14-3, Utah Geological Survey.
Paradis, O.P., 2019, Great Salt Lake Ooids: Insights into Rate of Formation, Potential as Paleoenvironmental Archives, and Biogenicity: Ph.D. Dissertation, University of Southern California.
Paul, D.S., and Manning, A.E., 2002, Great Salt Lake Waterbird Survey Five-Year Report, 1997-2001: Utah Division of Wildlife Resources, No. 08-38.
Purdy, E.G., 1963, Recent Calcium Carbonate Facies of the Great Bahama Bank, Sedimentary Facies: The Journal of Geology, 71(4), 472–497.
Roduit, N., 2019, JMicroVision: Image analysis toolbox for measuring and quantifying components of high-definition images, Version 1.3.1. https://jmicrovision.github.io (accessed 5 April 2019).
Rohweder, J., Rogala, J.T., Johnson, B.L., Anderson, D., Clark, S., Chamberlin, F., and Runyon, K., 2008, Application of Wind Fetch and Wave Models for Habitat Rehabilitation and Enhancement Projects: Open-File Report 2008–1200, USGS.
Schofield, I., Jewell, P., Chan, M., Currey, D., and Gregory, M., 2004, Shoreline development, longshore transport and surface wave dynamics, Pleistocene Lake Bonneville, Utah: Earth Surface Processes and Landforms, 29(13), 1675–1690.
Smith, B.P., Ingalls, M., Trower, E.J., Lingappa, U.F., Present, T.M., Magyar, J.S., and Fischer, W.W., 2020, Physical controls on carbonate intraclasts: Modern flat pebbles from Great Salt Lake, Utah: Journal of Geophysical Research. Earth Surface, 125(11). https://doi.org/10.1029/2020jf005733
Tarboton, D., 2017, Great Salt Lake Bathymetry: Hydroshare.
Tripp, T.G., 2009, Production of magnesium from Great Salt Lake, Utah, USA: Natural Resources and Environmental Issues, 15, Article 10.
Trower, E.J., Lamb, M.P., and Fischer, W.W., 2017, Experimental evidence that ooid size reflects a dynamic equilibrium between rapid precipitation and abrasion rates: Earth and Planetary Science Letters, 468, 112–118.
Trower, E.J., Bridgers, S.L., Lamb, M.P., and Fischer, W.W., 2020, Ooid cortical stratigraphy reveals common histories of individual co-occurring sedimentary grains: Journal of Geophysical Research, Earth Surface, 125(7). https://doi.org/10.1029/2019jf005452
U.S. Army Corps of Engineers, 2002, Coastal Engineering Manual (No. EM-1110-2-1100).
Vanden Berg, M.D., 2019, Domes, rings, ridges, and polygons: Characteristics of microbialites from Utah's Great Salt Lake: The Sedimentary Record, 17(1), 4–10.
Winland, H.D., and Matthews, R.K., 1974, Origin and significance of grapestone, Bahama islands: Journal of Sedimentary Research, 44(3).
Wurtsbaugh, W.A., 2009, Biostromes, brine flies, birds and the bioaccumulation of selenium in Great Salt Lake, Utah: Natural Resources and Environmental Issues, 15(2), 1–13.
Wurtsbaugh, W.A., Gardberg, J., and Izdepski, C., 2011, Biostrome communities and mercury and selenium bioaccumulation in the Great Salt Lake (Utah, USA): The Science of the Total Environment, 409(20), 4425–4434.